INSTITUTE OF PHYSICS PUBLISHING and INTERNATIONAL ATOMIC ENERGY AGENCY NUCLEAR FUSION

Nucl. Fusion **45** (2005) S227–S238 doi:10.1088/0029-5515/45/10/S18

Overview of the FTU results

B. Angelini[1], S.V. Annibaldi[1], M.L. Apicella[1], G. Apruzzese[1], E. Barbato[1], A. Bertocchi[1], F. Bombarda[1], C. Bourdelle[2], A. Bruschi[3], P. Buratti[1], G. Calabrò[1], A. Cardinali[1], L. Carraro[4], C. Castaldo[1], C. Centioli[1], R. Cesario[1], S. Cirant[3], V. Cocilovo[1], F. Crisanti[1], R. De Angelis[1], M. De Benedetti[1], F. De Marco[1], B. Esposito[1], D. Frigione[1], L. Gabellieri[1], F. Gandini[3], L. Garzotti[4], E. Giovannozzi[1], C. Gormezano[1,a], F. Gravanti[1], G. Granucci[3], G.T. Hoang[2], F. Iannone[1], H. Kroegler[1], E. Lazzaro[3], M. Leigheb[1], G. Maddaluno[1], G. Maffia[1], M. Marinucci[1], D. Marocco[1], J.R. Martin-Solis[5], F. Martini[4], M. Mattioli[6], G. Mazzitelli[1], C. Mazzotta[1], F. Mirizzi[1], G. Monari[1], S. Nowak[3], F. Orsitto[1], D. Pacella[1], L. Panaccione[1], M. Panella[1], P. Papitto[1], V. Pericoli-Ridolfini[1], L. Pieroni[1], S. Podda[1], M.E. Puiatti[4], G. Ravera[1], G. Regnoli[1], G.B. Righetti[1], F. Romanelli[1], M. Romanelli[1], F. Santini[1], M. Sassi[1], A. Saviliev[7], P. Scarin[4], A. Simonetto[3], P. Smeulders[1], E. Sternini[1], C. Sozzi[3], N. Tartoni[1], D. Terranova[4], B. Tilia[1], A.A. Tuccillo[1], O. Tudisco[1], M. Valisa[4], V. Vershkov[8], V. Vitale[1], G. Vlad[1] and F. Zonca[1]

[1] Associazione Euratom-ENEA sulla Fusione, C.R. Frascati, 00044, Frascati, Roma, Italy
[2] Association EURATOM-CEA, Cadarache, F-13108, Saint Paul-lez-Durance, France
[3] Associazione EURATOM-ENEA-CNR sulla Fusione, Istituto di Fisica del Plasma, Milano, Italy
[4] Consozio RFX, Corso Stati uniti 4, I-35100, Padova, Italy
[5] Universidad Carlos III de Madrid, Avenida de la Universidad 30, 28911 Madrid, Spain
[6] ENEA guest
[7] A.F. Ioffe Physico-Technical Institute RAS, Polytechnichestaya 26, 194021 St Petersburg, Russian Federation
[8] Nuclear Fusion Institute, RRC Kurchatov Institute, 123182 Kurchatov Sq.1, Moskow, Russian Federation

E-mail: gormezano@frascati.enea.it

Received 9 December 2004, accepted for publication 16 March 2005
Published 6 October 2005
Online at stacks.iop.org/NF/45/S227

Abstract

An overview of the FTU results during the period 2003–4 is presented. A prototype ITER-relevant lower hybrid current drive (LHCD) launcher, the passive active multijunction, has been successfully tested ($f = 8$ GHz) showing high power handling and good coupling properties and current drive comparable to those of a conventional launcher. Effective electron and ion heating (via collisions) have been achieved with the 140 GHz ECRH systems up to 1.5 MW, as well as current drive (25 kA at $n_{e0} = 8 \times 10^{19}$ m^{-3}). The mitigation of disruptions has been studied with on-axis ECRH. Ion Bernstein wave studies have shown the importance of recycling in achieving improved confinement plasmas. Advanced tokamak scenarios are presented including repetitive pellet enhanced plasmas and electron internal transport barriers (e-ITBs). Very peaked density profiles have been achieved with a low speed vertical pellet injector located at about mid-radius on the high field side. The performance is comparable to that achieved with a high-speed horizontal pellet injector. Possible reasons for this behaviour are discussed, among them the presence of an 'MHD' drift once particles reach the $q = 1$ surface. The effect of peaked density profiles on confinement is discussed. Electron ITBs can be produced at high density in FTU with LHCD only and with the combined use of LHCD and ECRH: $T_{e0} = 6$ keV with $n_{e0} = 1.4 \times 10^{20}$ m^{-3} and $H_{97} = 1.6$. Turbulence is strongly reduced. Ions are heated by collisions with $\Delta T_i / T_i$ up to 35% showing that e-ITBs are not degraded by the electron–ion collisions. Particle pinch studies have been made at high densities in full current drive conditions where the Ware pinch plays no role. An anomalous inward pinch exists even at these high densities ($n_{e0} = 1.5 \times 10^{20}$ m^{-3}). Despite the absence of energetic particles in FTU, MHD spectroscopy has revealed high frequency modes (30–80 kHz) that might have consequences for burning plasmas.

PACS numbers: 52.55.Fa, 52.50.Sw

[a] Author to whom any correspondence should be addressed.

1. Introduction

Experiments on the Frascati Tokamak FTU, which is a compact high magnetic field device ($R = 0.93$ m, $a = 0.3$ m, B_t up to 8 T, I_p up to 1.6 MA), are aimed at developing advanced scenarios at fields and densities relevant to ITER operation as well as its supporting physics [1]. The heating and current drive systems, lower hybrid current drive (LHCD, $f = 8$ GHz), electron cyclotron resonance frequency (ECRF, $f = 140$ GHz) and ion Bernstein waves (IBWs, $f = 433$ MHz), mainly interact with electrons. Ion heating is produced by electron–ion collisions, as it will be in ITER. The advanced scenarios in FTU include plasmas with peaked electron density achieved with pellet injection (pellet enhanced plasmas: PEPs) and plasmas with peaked electron temperature profiles (electron internal transport barriers: e-ITBs). In this paper, we mainly discuss e-ITBs since the study of ion ITBs is not possible at present in FTU due to the lack of a direct ion heating system that is needed to establish the high ion temperature gradients generally associated with ion ITBs.

The new hardware installed since IAEA 2002 [2] includes a high field side pellet injector, a prototype LHCD launcher for ITER and the completion of the ECRH system to four gyrotrons. New diagnostics include an upgrade of turbulence measurements, the installation of fast electron bremsstrahlung (FEB) cameras and a new CO_2 multi-channel interferometer. Turbulence measurements on FTU are carried out using a two-channel poloidal correlation reflectometer [3, 4], which can work either in O-mode, for low-density plasmas, or in X-mode, for high density ones. This technique is systematically applied to advanced scenario regimes when plasma conditions are such that the waves can be reflected in the area of interest in the plasma. Two FEB cameras (one vertical, one horizontal) detect the hard x-ray (HXR) emission along several chords in the poloidal cross section emitted by fast electron tails in the energy range 20–200 keV generated by LH waves. Inversion of HXR provides information on the radial location of these fast electrons that generate the non-inductive current drive. Therefore, localization of LHCD can be estimated allowing comparison and benchmarking with LH deposition codes to be made, especially at high density when radial diffusion of fast electrons is less important. The new interferometer is based on an innovative 'scanning beam' technique [5]: two CO_2 beams are spatially swept at high frequency (HF) across the plasma cross section. In this way, the density is measured along 30 chords separated in time, and one density profile is reconstructed every $\approx 50\ \mu$s.

In this paper, the main new results from the FTU heating and current drive systems will be presented first. New features of advanced tokamak (AT) scenarios including e-ITBs at high density and PEP modes achieved with the vertical pellet injector will then be discussed. Finally, the issues of ITER supporting physics (transport studies including particle pinch results and MHD spectroscopy) will be summarized.

2. Heating and current drive systems

2.1. Lower hybrid current drive

The design of the launcher mouth for ITER is very challenging. In addition to withstanding the significant heating due to the large level of radiation and of neutron fluxes in ITER, the LHCD launcher will have to be located in the full shadow of the vessel port to avoid damage from escaping particle flow and will still have to achieve a high level of power handling and current drive efficiency. It has been proposed to insert one passive waveguide between each active waveguide, the so-called passive active multijunction (PAM) [6], in order to provide for the cooling of the launcher mouth. The passive waveguides have a depth of about a quarter wavelength and reflect the wave so as to construct the required $N_\parallel$ spectrum, although with a slightly reduced directivity compared to a conventional launcher. A clear conceptual advantage is to operate with very low density at the grill mouth, as it will be in ITER far from the plasma edge. A prototype PAM unit (see figure 1) has been successfully tested in FTU [7]. A power density up to 75 MW m^{-2} has been launched for as long as the power can be applied (0.9 s). Taking into account a frequency dependence of the power handling capability [8], this power density is equivalent to 47 MW m^{-2} for the frequency foreseen for ITER (5 GHz), about 1.5 times the value corresponding to the ITER design value (33 MW m^{-2}). A very low power reflection coefficient (around 1.5%) has been measured with the density in front of the launcher close to the cut-off value even with the grill mouth retracted 2 mm inside the port shadow [9].

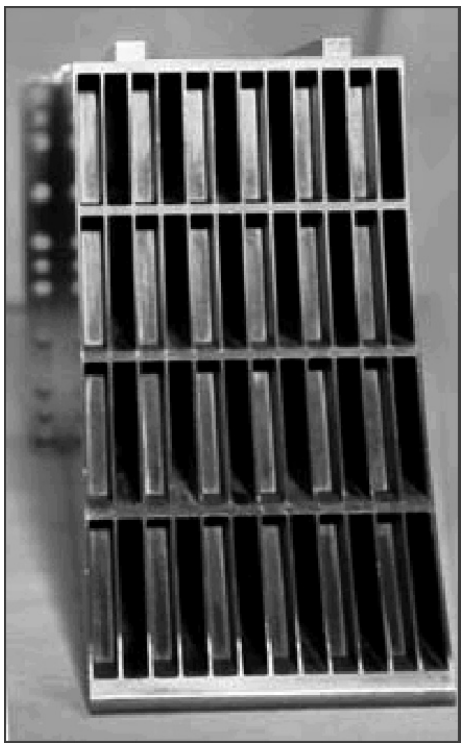

Figure 1. View of the PAM module for FTU (8 GHz).

The fast electron tail behaviour and the overall CD efficiency have been compared with those from a conventional grill launching a comparable $N_\parallel$ spectrum. Similar behaviour was observed [10]. The current drive efficiencies for a single PAM or a conventional grill module have been compared to the FTU database as shown in figure 2 where the LHCD efficiencies achieved in a variety of conditions have been plotted against $\langle T_e \rangle$. Since only one module has been used

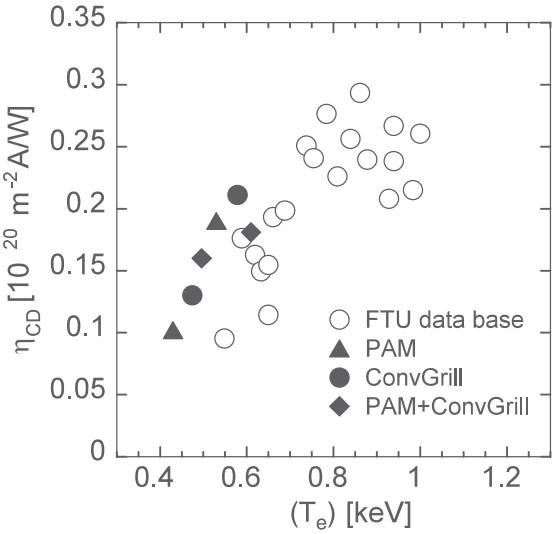

Figure 2. FTU database of current drive efficiency versus the volume averaged electron temperature $\langle T_e \rangle$. Open circles correspond to the conventional launcher up to its maximum power. Solid symbols correspond to the PAM antenna and to a conventional grill.

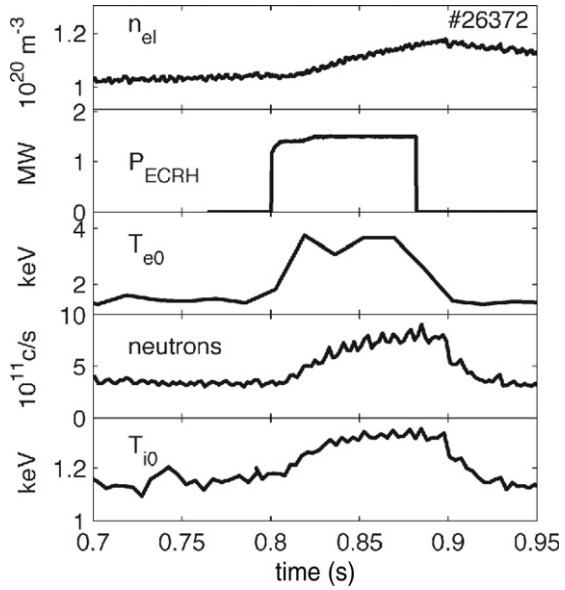

Figure 3. Time traces of the main signals of #26372 ($B_t = 5.3$ T, $I_p = 0.5$ MA). With 1.5 MW of ECRH power at $n_{e0} = 1.6 \times 10^{20}$ m^{-3}, T_e increases from 1.8 to 4 keV and the neutron rate is multiplied by ∼3 corresponding to $\Delta T_i/T_i = 25\%$. The increase of n_e is mainly due here to the ramping of the plasma current.

in this comparison, data corresponding to the PAM module are obtained in the low temperature range of the database. They fit very well with the other data. LHCD code simulations have been carried out using the FRTC ray tracing LHCD model (one-dimensional ($v_\parallel$) Fokker Planck package) [11] combined with the ASTRA code, that has been benchmarked already on FTU experimental data [12]. In the Fokker Planck model, *ad hoc* corrections to the collision operator that account for two-dimensional effects, such as pitch angle scattering as discussed in [13, 14], have modelled the FTU data reasonably well in reproducing the amount of non-inductive driven current as well as current density profiles (from fast electron HXR profiles) generated by LHCD. This LHCD modelling code, that has also been benchmarked on JET data, has been used for ITER modelling [15] both to reassess the LHCD frequency and to predict the LHCD efficiency in the context of an international effort [16][1].

2.2. Electron cyclotron resonance heating

The ECRF system of FTU is progressing to reach its nominal power level of up to 1.6 MW for 0.5 s with four 140 GHz microwave beams each focused by an independent mirror in a 4 cm spot, with a total maximum power density of 60 MW m^{-3}. In previous experiments [1], ECRH has been used in a large variety of applications, not only in plasma heating but also in the control of the power deposition profile allowing energy and particle transport to be studied under conditions directly relevant to ITER ($B_t = 5.3$ T, $n_e = 1 \times 10^{20}$ m^{-3}) as well as MHD control. Synergy between EC waves and LHCD will be discussed in section 3.2. In a first demonstrative short pulse (80 ms), ion heating through collisions from electrons, which was already observed at a power level of 0.8 MW [17], has been repeated at higher density: $n_{e0} = 1.6 \times 10^{20}$ m^{-3} with 1.5 MW of ECRF power. As shown in figure 3, T_{e0} increases from 1.3 to 4 keV and the neutron yield is increased by a factor 3, corresponding to $\Delta T_{i0}/T_{i0}$ of 25%. The ion temperature has been estimated from the maximum D–D neutron rate, assuming that deuteron and electron density profiles are similar. This assumption is justified by the small increase of the effective ion charge (Z_{eff} from ≈1.2 to 1.6), which affects, in a negligible way, the plasma dilution, in particular due to high Z elements such as molybdenum, the material of the FTU first wall. The neutron emission being mostly proportional to T_i^4 in this temperature range, the overall neutron emission came mainly from the plasma centre, and is, therefore, rather insensitive to the ion temperature profiles. The rise of the average density during the heating pulse is a common feature of all the FTU RF systems [12, 17] and it is mostly attributed to the increased gas flow from the limiter and vessel walls, while the contribution of the impurity influx is generally small for a cleaned machine, as discussed in [12]. The enhanced particle recycling, confirmed by the H_α radiation measurements, is caused by the larger thermal load and by the cryogenic temperatures of the FTU chamber (−100°C).

ECCD experiments have been performed at a power level of $P_{EC} = 1.1$ MW for 400 ms. In order to have a complete first-pass absorption, plasma parameters were selected to be $0.5 < \bar{n}_e < 0.6 \times 10^{20}$ m^{-3} and $3 < T_e < 5$ keV. The well-focused power density of 30–40 MW m^{-3} (strongly absorbed) leads to a parallel electric field $0.09 < E_\parallel/E_{cr} < 0.25$, E_{cr} being the electric field above which thermal electrons can run away [18]. Therefore, a linearized theoretical treatment is adequate. A series of experiments with the toroidal injection angle set at ±10°, ±20°, ±30° (off perpendicular) have permitted us to make a first assessment of the driven current in discharges with $I_p = 400$ kA and $2.5 < Z_{eff} < 3$. The EC driven current has been calculated both through the plasma resistance (using

[1] See also chapter 6 of the *Tokamak Physics Basis* (in preparation, to be submitted to *Nuclear Fusion*) being prepared by the ITPA Topical Group on Steady State Operation.

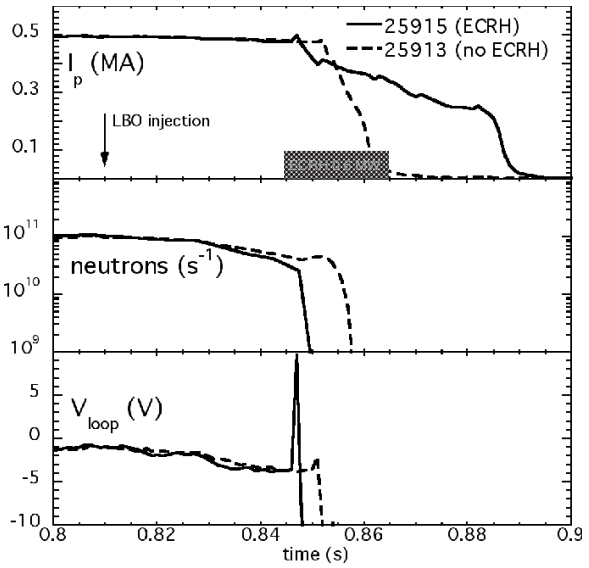

Figure 4. Application of central ECRH to disruptions triggered by injection of Mo through LBO comparing #25915 and #25913 with and without ECRH: decay of plasma current is lengthened, neutrons induced by runaways are reduced and the peak in loop voltage is suppressed.

neo-classical resistivity) and from comparison of co- and counter-experiments, considering the difference in $\Delta V_{\rm loop}$. $I_{\rm ECCD}$ values up to 15–20 kA (at the best angle of $\pm 20^\circ$) were obtained from both these methods. Considering the small amount of driven current (5–6% of $I_{\rm p}$), it is important to mention that these techniques have to be used very carefully. In particular, the calculation made by comparing co- and counter-injection can be affected by small differences in the plasma parameters between the two discharges. The calculation of the plasma resistance is also very sensitive to the estimation of $T_{\rm e}$, $n_{\rm e}$ and $Z_{\rm eff}$ profiles (the latter being assumed constant in our calculations). However, the agreement between these measurements and the linear theory by using the beam tracing ECWGB code [19] is within $\pm 10\%$, already a satisfactory output for these very first experiments in FTU.

The observation that, in FTU, a drop in plasma resistivity (and, in turn, in the toroidal electric field) due to ECRH leads to runaway suppression during the plasma current plateau [20], has initiated the testing of a such a scheme as a technique to mitigate disruptions by changing the resistivity of the plasma through on-axis EC heating. An experiment has been carried out in which controlled disruptions ($I_{\rm p} = 500$ kA, $B_{\rm t} = 5.3$ T) have been triggered by injection of impurities (typically Mo) through laser blow-off (LBO). ECRH pulses of 20–100 ms duration have been started within a few milliseconds before the time of the disruption, as shown in figure 4. As a result, the current decay is much lengthened and neutrons (from runaways) are reduced: low or no γ-ray peaks (measured with a NE213 scintillator running in current mode with a time resolution of 50 μs) due to disruption-generated runaways are observed at an ECRH power level of 0.65 MW. Without ECRH such a reduction in runaway-induced gamma rays is not observed. The preliminary results indicate that an ECRH power as low as 35% of the Ohmic power produces a softening of the plasma current decay (i.e. longer decay) and, in several cases, even prevents the disruption when ECRH application is early enough with respect to the disruption time. The loop voltage generally increases to a very high level prior to the disruption: a feedback system using this effect is being prepared to mitigate disruptions in FTU in a controlled way.

2.3. Ion Bernstein waves

As reported in [1, 21], 0.4 MW of IBW power was coupled in a deuterium plasma at $I_{\rm p} = 0.8$ MA, $n_{\rm e} = 0.5 \times 10^{20}$ m^{-3} and $B_{\rm t} = 7.9$ T. Some increase in the electron pressure profile peaking factor (20%) was found accompanied by a decrease of the electron thermal conductivity by 40% over the radial region inside the expected IBW deposition layer. Additional experiments were performed in 2003 under similar conditions. However, no pressure peaking during IBW power application was observed. The cause of this difference remains to be established. In contrast with older experiments, higher impurity content (Mo, O) and a higher recycling (D_α being a factor 2 higher) were observed. Therefore, one possible explanation is a spurious absorption of the wave in the scrape-off plasma, although, since the Langmuir probes were being perturbed by the IBW wave, it was not possible to document such an effect. Further experiments will be performed in cleaner plasmas with lower recycling in order to fully assess the role of the IBW power injection in producing confinement improvement. Reflectometry measurements have been carried out so far only for a set of discharges in which the improved core confinement could not be reproduced. However, even under these conditions, turbulence measurements have shown that some reduction in the turbulence level occurs during IBW injection [22]. Using O-mode reflectometry measurements, two sets of discharges have been compared, with and without IBW, showing that inside the absorption layer ($r/a \approx 0.55$) the quasi-coherent (QC) component of the turbulence [23, 24] is reduced by about 40%, while the self-correlation time of the turbulence increases (but not the self-correlation length). A reduction in the poloidal speed for the QC component is also observed but not for the low frequency one. Instead, a reduction of the low frequency component is observed close to the absorption layer ($r/a \approx 0.7$). The value of $k_\theta \rho_{\rm i}$ (about 0.3) of the QC modes is compatible with ITG turbulence. Here k_θ is defined as $\Omega_{\rm QC}/v_\theta$ where $\Omega_{\rm QC}$ is the frequency of the mode and v_θ is the poloidal velocity of the turbulence as measured by the two channel cross correlation.

3. Advanced tokamak scenarios

3.1. Improved performance plasmas with pellet injection

High-density plasmas with peaked density profiles have been achieved in FTU with multiple pellet injection from a high-speed horizontal pellet injector capable of injecting up to 5 deuterium pellets per discharge, at 2 km s^{-1} [25]. Transient improved core confinement plasmas with very low $Z_{\rm eff}$ have led to record values in FTU for the neutron yield and for $n_{\rm i}\tau_E T_{\rm i}$ (0.8×10^{20} m^{-3} keV s^{-1}). The achievement of repetitive PEP mode phases following the injection of up to 5 pellets at intervals of about 100 ms has maintained the average D–D neutron yield a factor 2–3 higher than was achieved with

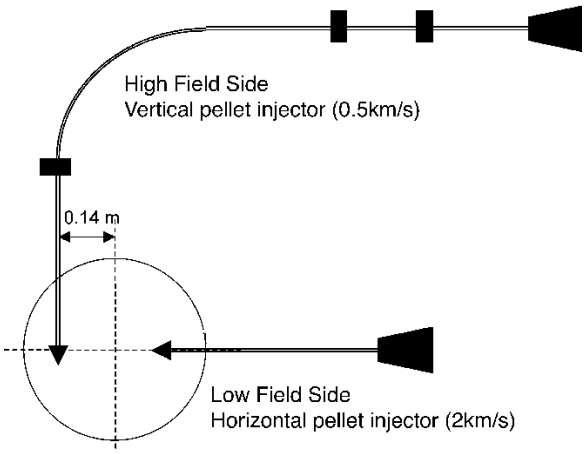

Figure 5. Sketch of the two pellet launchers installed on FTU.

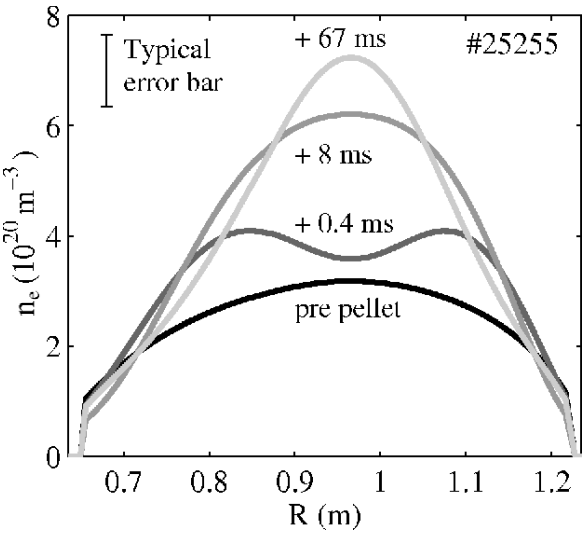

Figure 6. Density peaking following vertical pellet injection (from the CO_2 multi-channel interferometer). Times refer to the start of pellet injection. Particle 'magnetic' pinch is estimated to take place at around $t = 0.4$ ms. A typical error bar is also indicated.

gas fuelling throughout the current plateau. A large central density peaking was observed although pellets were mostly ablated at about mid-radius. Detailed analysis of the data [26] has shown that pellet ablation near the $q = 1$ surface triggers the fast growth of an $m = 1$ magnetic island: as the island reaches a large amplitude, magnetic reconnection mixes the plasma centre with the $q = 1$ pellet fuelled region, thus enhancing the effective pellet deposition depth. This effect was well reproduced by MHD codes [27].

As shown in figure 5, a new vertical pellet launcher has been installed to feed a vertical injection line displaced towards the high toroidal field side at a radius of $r/a \sim 0.6$ [28]. Pellets have been injected along a guide system with only one bend (3 m radius) allowing velocities up to 0.5 km s^{-1} to be achieved. In spite of the geometry of the pellet launch, a large peaking of the plasma density is routinely observed as illustrated in figure 6. A first phase, for about 0.3–0.4 ms, follows the ablation of the pellet where the ablated particles reach the $q = 1$ surface. The possible role of an electric radial drift due to $\nabla B/B$ is discussed in [29]. Then, an $m = 1$ island is formed and particles are rapidly advected towards the plasma centre. The density profile evolves from a hollow profile, as confirmed by means of Thomson scattering measurements done 0.3–0.5 ms after pellet injection, to a peaked profile with the central density reaching (7–8) $\times 10^{20}$ m^{-3}. Following this MHD event, the density profile continues to peak slowly for the full duration of the PEP mode: here ∼70 ms, about one τ_E. Mild sawtooth activity, such as shown in figure 7, generates a small decrease in the central density. In turn, this prevents accumulation of impurities.

Sometimes, an $m = 2$ mode is triggered after pellet injection, preventing the formation of a subsequent PEP and leading in some cases to a disruption. It has been shown that this is caused by an excessive amount of light impurities (oxygen) leading to a change in the current profile. In this case, the subsequent turbulence level is high, confirming the absence of a PEP [30]. Clean machine conditions avoid this effect and multiple PEP modes were achieved with performance similar to the multiple PEP modes achieved with the horizontal launcher, as shown in figure 7, in spite of the large distance between the tangential line and the plasma centre. Performance is characterized by a strong reheat of the electrons to the pre-pellet level and the achievement of neutron yield levels that exceed 1×10^{13} counts s^{-1}, which are in the range of record values in FTU, the detailed behaviour of the neutron yield depending upon the sawtooth activity. In this series of experiments, the number of pellets from the vertical pellet launcher was technically limited to 2–3 successive pellets.

Some systematic studies have been done to assess the role of the initial drift by comparing 0.8 and 1.1 MA PEPs at 7.2 T and, therefore, with different distances between the injection of the vertical pellet and the $q = 1$ magnetic surface [29]. At 1.1 MA, PEPs are robust and can be produced in a large range of plasma conditions. At 0.8 MA, PEPs are not produced when the target temperature is too low, probably due to the fact that the pellet passes through the plasma without being fully ablated, and to the too large distance between the $q = 1$ surface and the vertical pellet. When the target temperature is higher, a PEP can be formed. However, in contrast with the horizontal pellet injection, no prompt island formation is observed and the density peaking takes place on a longer time scale due to a combination of sawteeth and particle pinch, as discussed in [29].

This increased evidence of the 'MHD' pinch might alleviate some of the constraints of pellet fuelling in devices such as ITER since ablation has only to take place at a reasonable distance from the $q = 1$ magnetic surface in order to fuel the plasma centre.

3.2. Electron internal transport barriers

Improved confinement plasmas with the production of e-ITBs have been achieved in the current ramp-up phase of FTU ($B_t = 7.0$ T, $I_p = 0.8$ MA, $P_{LHCD} \approx 0.7$ MW) with LHCD only. Such barriers have been seen in many other experiments, although at generally low densities: $n_e = (0.7–2) \times 10^{19}$ m^{-3}. In FTU, such e-ITBs with LHCD only have been produced at higher densities, as shown in figure 8. Plasmas with 8 keV electron temperature, at densities up to 6×10^{19} m^{-3}, have

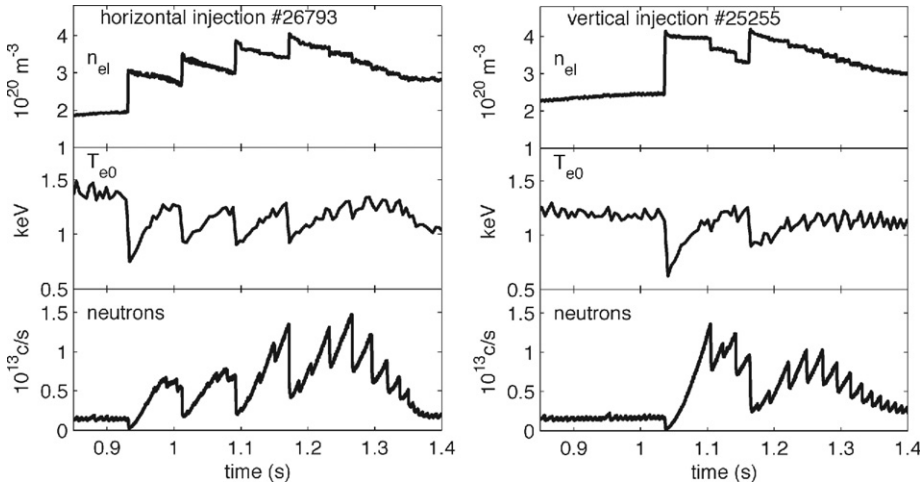

Figure 7. Comparison of multiple PEP modes achieved with the horizontal (#26793) and the vertical (#25255) pellet injectors at $B_t = 7.2$ T with $I_p = 1.1$ MA. n_{el} refers to the line averaged density.

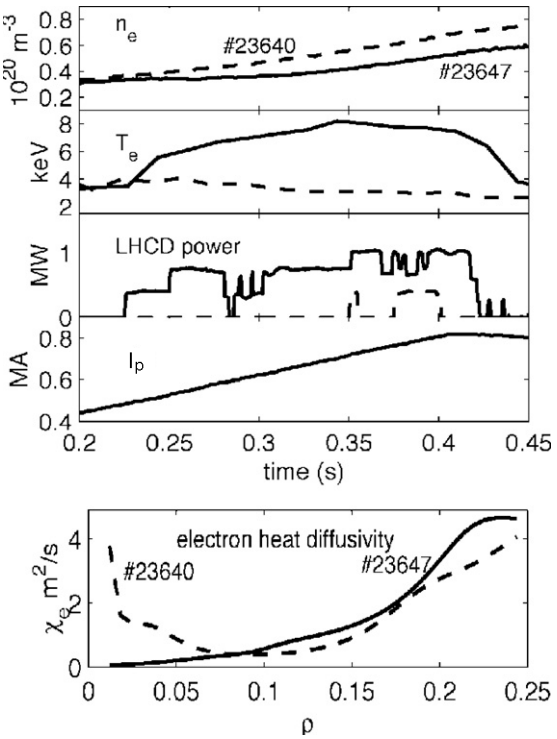

Figure 8. Main signals of an improved confinement discharge (#23647 at $B_t = 7$ T, ——) compared with a similar discharge without LHCD (#23640, - - - -). Comparison of the respective χ_e (at $t = 0.4$ s) shows an improved confinement (from $r = 2$ cm, the temperature gradients are sufficiently high to produce reliable results, the Thomson scattering system giving a temperature measurement every 2 cm starting from the plasma centre). The LHCD power was not maintained due to coupling problems in the transition from the ramp-up to the plateau phase.

been achieved in the ramp-up phase of a 7.9 T/0.8 MA plasma [31]. The absence of any effect when a second short LH pulse is applied in #23647 is due to the combined effects of a higher density and a higher plasma current that reduce by more than three times the fraction of the non-inductive current driven by LHCD and its subsequent change of the current profile. Comparison of electron heat conductivities, calculated from the JETTO code [32], between an improved confinement discharge and a similar discharge without LHCD shows that central values of χ_e are reduced by more than an order of magnitude. However, the volume of the improved confinement region is too small to produce a significant improvement in the global confinement. Improved LHCD coupling techniques have to be developed to maintain the ITB during the plateau phase in order to benefit from the improved LHCD efficiency at this high magnetic field.

Improved confinement plasmas at ITER relevant parameters ($B_t = 5.3$ T, $n_e \approx 10^{20}$ m^{-3}) in FTU are normally achieved with combined LHCD and ECRF in magnetic configurations with a flat or mild negative shear, similar to the one corresponding to advanced scenarios planned for ITER. Central electron temperatures in excess of 6 keV, together with central densities up to 1×10^{20} m^{-3} and H_{97} factors up to 1.6, have been reported in [33, 34]. More recently, e-ITBs have been produced at even higher densities as shown in figure 9(*a*). Central electron temperatures of 5–6 keV have been maintained for $n_{e0} = 1.4 \times 10^{20}$ m^{-3} for as long as the power (1.5 MW LHCD and 1.1 MW of ECRF power) was applied in the plateau phase of 5.3 T/0.4 MA discharges. The existing weak sawteeth activity disappears immediately when power is applied and no significant MHD activity was noted in these discharges. The corresponding electron temperature profiles are given in figure 9(*b*) showing a significant improvement in the whole plasma radius. A change in the electron temperature gradient is observed to take place at about $r/a = 0.3$. Assuming that an ITB is formed [34] when the maximum value of the quantity $\rho_T^* = \rho_{L,s}/L_T$ (indicative of the normalized temperature gradient) becomes larger than a threshold value of 0.014, similar to the one that has been found in JET [35], an ITB is formed at $r/a \sim 0.3$. $\rho_{L,s}$ is the Larmor radius of the ions moving at sound velocity and $L_T = T_e/(dT_e/dr)$ is the local characteristic length for the variation of the electron temperature. In the discharge #26671 shown in figure 9, the ITB has been maintained for about $20\tau_E$ with an H_{97} factor of 1.6 as estimated from the JETTO code. The calculated current profile is rather flat with q-values of about 1.2 in the inner part of the plasma and is slightly reversed close to the plasma centre with q_0 increasing progressively

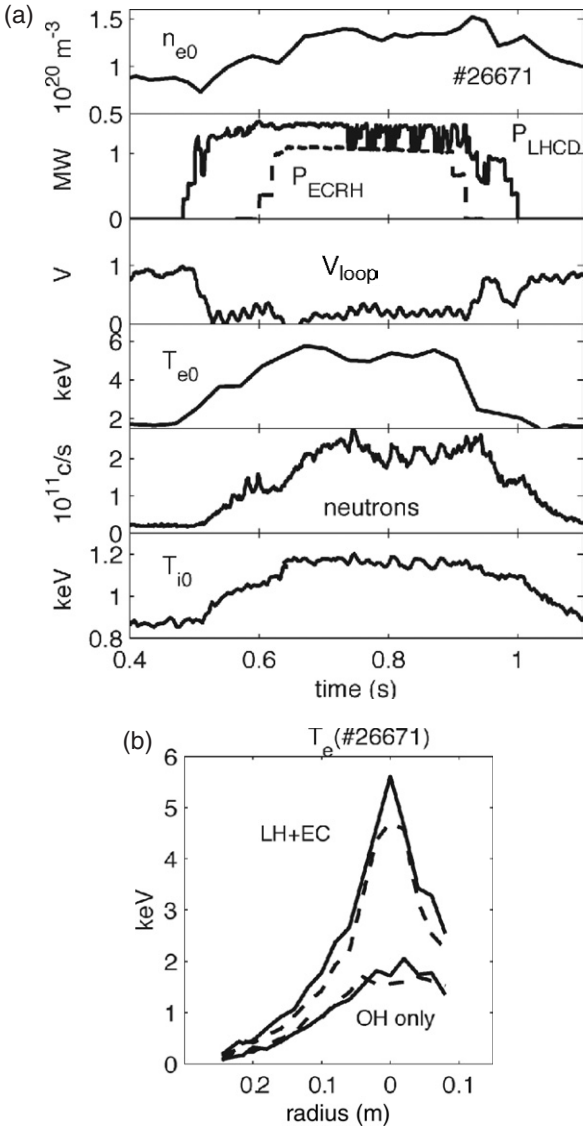

Figure 9. (*a*) Main signals of #26671: $B_t = 5.3$ T, $I_p = 0.4$ MA. The central density is from the scanning CO_2 interferometer. The ion temperature is calculated using neutron and density profiles. (*b*) Electron temperature profiles in #26671 from Thomson scattering during the Ohmic phase: 0.4 s before heating (——) and 1.1 s in the post-heating phase (- - - -); and during the main heating phase: 0.6 s (——) and 0.7 s (- - - -).

from 1.2 to 1.6. These calculations are performed using the radial profiles of the HXRs emitted perpendicularly to the toroidal magnetic field by the LHCD generated fast electrons. As discussed in the introduction, this technique to estimate the LHCD power deposition is quite reliable because the radial diffusion of fast electrons is negligible at these high densities, in particular when the ratio I_{LH}/I_p is large (low residual electric field and low Ohmic current). Moreover, the calculated current profile is confirmed by the clear observation of a $(m, n) = (3, 2)$ MHD double tearing mode (detected by a set of Mirnov coils), indicating a double crossing of the $q = 1.5$ magnetic field line at the anticipated locations.

Using the reflectometer, turbulence was analysed by comparing pulse #26669, where an ITB was formed, with a similar pulse (#26672), where an ITB was not formed due to the lack of ECRH power (see figure 10(*a*)), under conditions where the wave was reflected at about the same radius. A reduction of the turbulent spectra both in the low frequency band and in the broadband range is observed as shown in figure 10(*b*). This is associated with the disappearance of the cross-correlation between the two poloidal channels. The width of the auto correlation is also much reduced. It is interesting that a similar observation was made in T-10 during the formation of an e-ITB with ECRF [36]. It is, therefore, likely that this reduction in the turbulence spectrum is intrinsic to the production of e-ITBs.

In figure 9(*a*), it can be seen that the neutron yield increases by one order of magnitude when the power is applied. Since both LHCD and ECRH deliver their power to the electrons, ions are heated via collisional power transfer from electrons: from the D–D neutron increase, we infer $\Delta T_{i0}/T_{i0} \sim 35\%$. In this discharge, the ion temperature profile has been determined by using the emissivity profiles of the neutron camera (6 radial chords) and the density profiles. Transport analysis with JETTO using such T_i profiles as input shows that the experimental ion conductivity is reduced to values close to neo-classical levels ($\chi_i \approx 0.1\,m^2\,s^{-1}$) inside the ITB radius. This result is consistent with previous analyses [34, 37], in which (as T_i profiles were not available) ion transport was inferred by modelling it as a multiple of neo-classical transport (spatially constant) and adjusting the multiplier to match the overall neutron rate. Global ion behaviour can be inferred by comparing the ion thermal energy density and the power transferred to ions by collisions with electrons in the volume inside the ITB radius. The observed relationship between these two quantities is linear and is a good indication that ions are efficiently heated from direct collisional heating. The corresponding incremental ion energy confinement time in the plasma core, $\tau_{E,\mathrm{iincr}} \approx 24.6$ ms, is comparable to or larger than the global energy confinement time, on average 20 ms [34]. However, the ratio between the thermal equipartition time and energy confinement time remains at about a factor 5–8. Therefore, although this is a first indication that ion–electron collisions are compatible with e-ITBs, a clear demonstration of this point would require operation with higher energy confinement, probably at higher plasma current and, therefore, with higher additional power.

Electron ITBs at high densities and higher magnetic field have also been produced using a possible synergy between ECRF and LHCD. At $B_t = 7.2$ T, the 'cold resonance' for ECRF is outside the plasma. The EC wave is absorbed by the fast electron tail generated by LHCD through Doppler shift [17]. This effect was already documented in FTU [2]. In more recent experiments, this effect has been used to enhance the current drive generated by LH waves. Almost full current drive was achieved at $B_t = 7.2$ T, $I_p = 0.5$ MA and $n_{e0} = 0.9 \times 10^{20}\,m^{-3}$ with 1 MW of LHCD and 1.1 MW of ECRF power. The HXR signal from the FEB camera (50–200 keV) was doubled when ECRF was applied. As shown in figure 11(*a*) an ITB was triggered by this Doppler-shifted EC resonance during the ramp-up phase of a 7.2 T/0.8 MA pulse at a central density in excess of $n_{e0} = 1.0 \times 10^{20}\,m^{-3}$, as shown from the electron temperature profiles (figure 11(*b*)). The radial inverted HXR signals from the FEB camera (20–100 keV) are shown in figure 11(*c*). The discussion of the influence of the plasma density on the

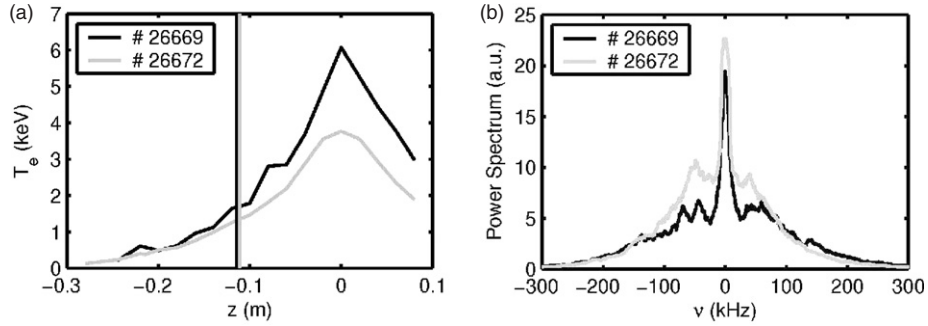

Figure 10. (*a*) Electron temperature profiles at $t = 0.7$ s for #26669 with LHCD and ECRH power (black line) and for #26672 with LHCD only (grey line) in which an ITB is not formed. Both pulses are at 7.2 T and 0.4 MA and the same initial density. The vertical line indicates the radius of reflection for the reflectometry. (*b*) Turbulent spectra from the reflectometer for #26669 (with ITB, black line) and #26672 (without ITB, grey line), both at 0.7 s. The low frequency (LF) component is the peak between −20 and +20 kHz whereas the QC component has its peak at about 70 kHz. Both measurements were taken at r/a of about 0.4, which is just about the barrier foot.

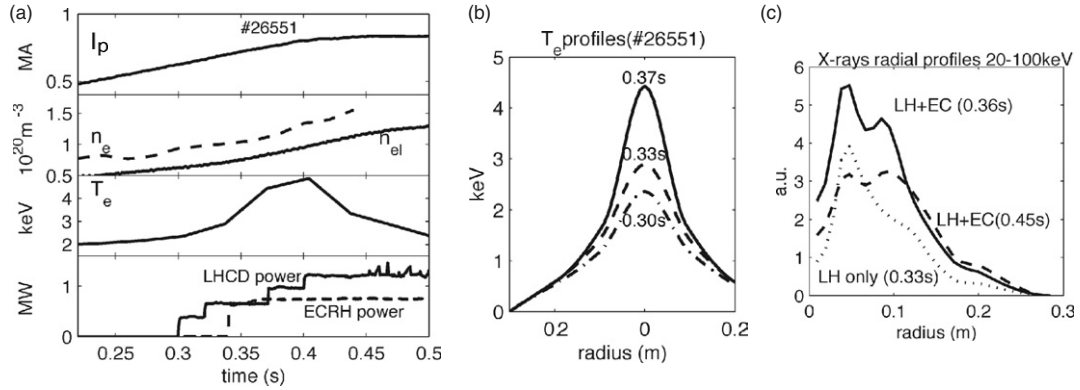

Figure 11. (*a*) Main signals of #26551. LHCD and ECRF are applied during the ramp-up phase of a 0.8 MA, 7.2 T pulse. 'Cold' EC resonance is outside the plasma. An ITB is not maintained when the density increases at too high a rate. Plotted densities are the line-averaged density ($n_{\rm el}$) and the central density ($n_{\rm e0}$). (*b*) Electron temperature profiles (from Thomson scattering) in #26651 during the pre-heat phase ($t = 0.30$ s, — · —), the start of EC + LHCD phase ($t = 0.33$ s, - - - -) and at $t = 0.37$ s (——) when the ITB starts to collapse when the density is too high. (*c*) Radial inverted HXR signals from the FEB camera for #26651 during the LHCD only phase ($t = 0.33$ s, · · · · · ·), the start of EC + LHCD phase ($t = 0.36$ s, ——) and at $t = 0.45$ s (- - - -) when the ITB starts to collapse when the density is too high. There is an integration time of about 20 ms.

HXR spectra is a complex issue that depends upon the launched $N_\parallel$ LH spectrum, the toroidal up-shift of the launched LH waves and also upon the poloidal launching angle and the collisional scattering of the fast electron population as well as the available LH power. Although a clear effect of the plasma density on these profiles has not been observed so far, such a discussion is beyond the scope of this paper. When ECRF is applied, spectra are initially substantially enhanced but are subsequently reduced. When the density increases during the current ramp-up phase, the energetic electron population is affected in such a way that the damping of the EC waves via Doppler shift is less effective. As a result, the amount of non-inductive current drive is reduced and, since the plasma current is ramped up, the plasma current is less and less modified resulting in the loss of the ITB for the available power. At $t = 0.36$ s, the power coupled to the fast electrons is estimated to be about 50% of the ECRH power. When the density increases further, the LHCD power (1.3 MW) is not large enough to maintain a sufficient electron energetic tail and the coupled EC decreases (by about 40%), the HXR spectrum reduces and the ITB cannot be maintained. Higher power would be necessary to maintain e-ITBs in these high density/high current plasmas.

4. Supporting physics

4.1. Heat transport analysis

A study of the confinement properties of FTU plasmas including advanced scenario (i.e. multiple pellet fuelled, e-ITBs and RI modes [38]) discharges is carried out in FTU by means of transport code analysis (JETTO), q being spanned from roughly 2 to 6. In the analysis, electron transport is determined experimentally from energy balance, while ion transport is based on a neo-classical model. The measured τ_E in Ohmic discharges is found to be $\sim 0.92 \times \tau_{E\rm ITER97}$ and the linear trend with the line-averaged density saturates at a value of ∼50 ms for $\bar{n}_{\rm e} > 0.5 \times \bar{n}_{\rm Greenwald}$ ($\tau_{E\rm ITER97}$ being the ITER97 L-mode scaling [33]). Standard L-modes (with ECRH, IBW and LH additional heating) as well as RI mode discharges are in good agreement with the ITER97 L-mode scaling predictions. An improvement of τ_E up to 60% with respect to the ITER97 L-mode scaling is found for additionally heated discharges (LH plus ECRH or LH only) in which ITB formation has occurred.

Transport analysis of a set of 7.2 T Ohmic discharges was performed in order to investigate the effect of pellet injection

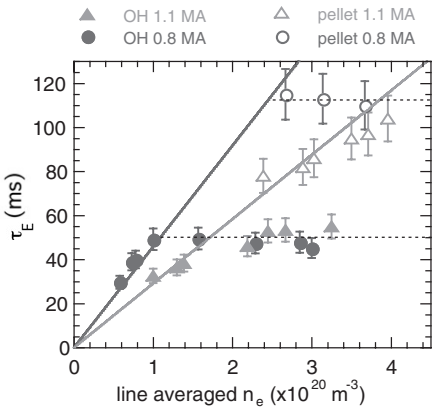

Figure 12. Energy confinement time versus line-averaged density in FTU. The saturation observed with gas-fuelling is removed in pellet-fuelled plasmas due to the density peaking. A second saturation is observed at high density.

on the energy confinement time (τ_E) [30, 33] in plasmas with $T_e \sim T_i$. The linear phase of τ_E versus the line-integrated density ($\bar{n}_e$) can be described as

$$\tau_E^{\text{linear}}\ (\text{ms}) = k\bar{n}_e q^{1.42\pm0.07}$$

($\bar{n}_e$ is in units of 10^{20} m^{-3}, q is the cylindrical safety factor and k is a constant). A saturation of τ_E with increasing density is observed, which can be related to the change from the electron to the ion transport dominated regime at high density. The linear dependence of τ_E on $\bar{n}_e$ is recovered, although transiently, when peaked density profiles are achieved as a result of pellet fuelling. The improvement of confinement with pellet fuelling corresponds to a strongly reduced χ_i (neo-classical level) as compared with the one in the gas-fuelled case at the same density, whereas electron transport in this phase is again dominant. This is in qualitative agreement with theory [39], which predicts the suppression of ion temperature gradient modes with density peaking. However, recent experiments with pellet injection at $n_e > 2 \times 10^{20}$ m^{-3} at $I_p = 0.8$ and 1.1 MA have shown that a second saturation is observed as indicated in figure 12. This second saturation occurs when the electron conductivity reaches the same level as the ion neo-classical conductivity [40].

4.2. Particle pinch

Particle transport will have a large impact on the density profile in ITER, where central fuelling will be negligible, in influencing the density profile and, consequently, the overall confinement. The particle flux, including turbulent transport [40, 41], can be written as

$$\Gamma = -D[\nabla n + C_q \nabla q/q\, n - C_T \nabla T_e/T_e\, n] + V_{\text{Ware}} n$$

D being a turbulent diffusion coefficient. The so-called Ware pinch, or neo-classical pinch, is mainly driven by the toroidal electric field. It is, therefore, of particular interest to assess such a pinch effect in experiments with full non-inductive current drive leading to a null toroidal electric field with only RF heating and current drive techniques, without any internal fuelling.

The existence of an anomalous inward pinch in steady-state plasmas without an electric field was demonstrated in Tore Supra [42]. However, such a demonstration was done at rather low density: $n_{e0} = (2\text{–}3.5) \times 10^{19}$ m^{-3} (with $T_{e0} = 4.8$ keV). A similar set of experiments has been done in FTU under conditions of higher density and collisionality more relevant to ITER, as shown for example in figure 13(*a*). Full current drive conditions were achieved with 1.5 MW of LHCD for the following conditions: $B_t = 7.2$ T, $I_p = 0.5$ MA, $n_{e0} = 1.5 \times 10^{20}$ m^{-3} and $T_{e0} = 6\text{–}4$ keV for about $10\tau_E$, followed by almost full current drive ($\Delta V_{\text{loop}}/V_{\text{loop}} = 90\%$ with $V_{\text{loop}} = 0.1$ V) for a further $10\tau_E$. Electron collisionality at the plasma centre, ν_e^*, is about 0.1. The normalized density profile flattens significantly during the quasi-full current drive phase, as shown in figure 13(*b*), but remains peaked. The profile remains unchanged during the full duration of the quasi-full current drive phase. Data analysis [30] confirms the results found in Tore Supra at a lower collisionality, as shown in figure 14, where the density peaking is plotted against the temperature gradient in the inner part of the plasma. Further analysis of these results, taking into account those recently achieved in Tore Supra [43], and assessment of their consequence for ITER is underway.

4.3. MHD spectroscopy

HF oscillations that accompany the development of $m = 2$, $n = 1$ islands have been observed in Ohmic plasmas [44]. HF oscillations appear above a threshold island amplitude corresponding to an $m = 2$ edge poloidal field relative perturbation of 0.2%. A typical spectrogram of these HF oscillations is shown in figure 15. Several pairs of HF lines can be observed between 30 and 70 kHz; each pair merges into a single line as the island frequency decreases to zero. Poloidal and toroidal mode numbers (m, n) have been measured for the pair lying between 40 and 50 kHz; the upper line has $(-2, -1)$ and the lower one has $(2, 1)$. The frequency range of HF modes is inside the low frequency gap introduced in the shear Alfvén continuous spectrum by finite beta effects [45], while the toroidicity induced gap [46] is one order of magnitude higher. Since there are no fast ions that can excite Alfvén modes, the observed perturbations are likely to be due to the nonlinear excitation of shear-Alfvén waves by the magnetic island. More precisely, we conjecture that modes of the beta induced Alfvén eigenmode (BAE) branch [45] are nearly marginally stable in the case under investigation, and can be nonlinearly excited in the presence of a sufficiently large magnetic island. These modes are kinetic interchange waves, which are radially localized about their mode rational surface [47]. The lowest order BAE angular frequency can be estimated by

$$\omega \cong \frac{1}{R}\sqrt{\frac{2T_i}{m_i}}\left(\frac{7}{4} + \frac{T_e}{T_i}\right)^{1/2},$$

i.e. by the accumulation point of the low frequency gap introduced in the shear Alfvén continuous spectrum because of finite beta [47]. This frequency is an upper bound for the expected mode frequencies, consistent with experimental observations. Pairs of BAEs, with given helicity and localized near the $q = 2$ surface, can interact with the $(2, 1)$ mode

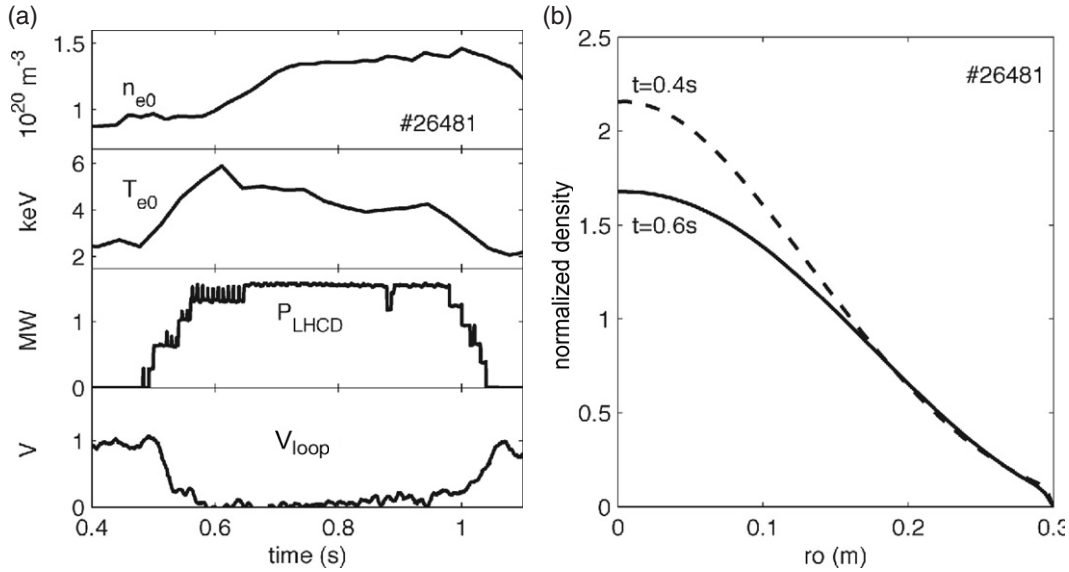

Figure 13. (*a*) The main signals of a full current drive discharge (#26481) at high density ($B_t = 5.3$ T, $I_p = 0.5$ MA). Zero loop voltage is maintained from $t \sim 0.6$ to 0.8 s. (*b*) Density profiles normalized to the volume averaged density ($n_e/\langle n_e \rangle$) for #26481 during the pre-heat phase ($t = 0.4$ s, - - - -) and during the full current drive phase ($t = 0.6$ s, ——). Normalized profiles remain similar from 0.6 to 0.9 s.

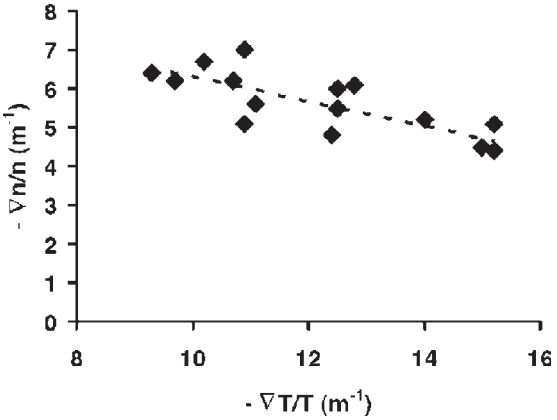

Figure 14. Dependence of $\nabla n/n$ on $\nabla T/T$ for a series of pulses with full current drive: #22424, #21638 and #26481. The data reported are taken at three radial positions: $r = 10$ cm, 12 cm and 15 cm corresponding, respectively, to $r/a = 0.33$, 0.4 and 0.5.

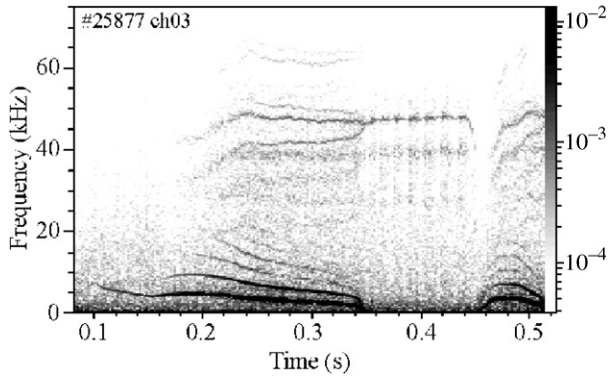

Figure 15. Spectrogram of a Mirnov coil for #25877. Ordinates and grey scales indicate frequency and amplitude, respectively. Intense lines below 20 kHz correspond to the (2, 1) tearing mode and its harmonics while lines above 30 kHz correspond to the HF waves.

via three-wave couplings and be nonlinearly excited provided that the energy transfer rate from the (2, 1) island to BAEs is sufficient to overcome the linear mode damping, thereby setting a threshold condition for the island amplitude. For example, a $(-4, -2)$ and (2, 1) BAE pair can nonlinearly interact with the $(-2, -1)$ tearing. Note that negative mode numbers, in the present convention, correspond to modes propagating in the electron diamagnetic direction, like the tearing mode. For each BAE propagating in the electron diamagnetic direction, the model discussed in [47] predicts that there will be a twin BAE wave propagating in the ion diamagnetic direction. However, as discussed earlier, they are not these twin waves that form the BAE pair nonlinearly interacting with the tearing mode via three-wave couplings. Detailed theoretical studies are underway, providing the formal analytical support for our conjecture and its benchmark against experimental results. At present, it can be stated that this conjecture is in qualitative agreement with observations and provides an explanation of the dominant (2, 1) and $(-2, -1)$ HF modes shown in figure 15. In fact, assuming that these modes are BAEs, as discussed earlier, they ought to be radially localized at about the $q = 2$ surface, as would other nonlinearly excited BAEs. Lower mode numbers, then, have higher amplitude at the plasma edge and dominate the Mirnov coil spectrum. At the lowest order, the (2, 1) and $(-2, -1)$ HF modes are degenerate in the plasma frame. However, in the presence of finite plasma rotation, the $(-2, -1)$ mode accelerates while the (2, 1) slows down, till mode-locking sets in and the mode frequency becomes degenerate once more. The impact of such HF modes on burning plasmas is being assessed.

5. Conclusions and perspectives

Substantial progress has been made since the IAEA Fusion Energy Conference in Lyon, France (2002). In addition to

investigating several physics issues, notably IBWs and HF Alfvén type MHD modes, very peaked density profiles have been achieved with a low speed vertical pellet injector located at about the mid-radius on the high field side confirming the presence of an 'MHD' drift once particles reach the $q = 1$ surface. Performance with the vertical pellet injector is comparable to that achieved with a high-speed horizontal pellet injector. Peaked density profiles allow a linear dependence of τ_E with density to be recovered but saturation at higher values of τ_E remains.

Effective electron and ion heating (via collisions) have been achieved with the 140 GHz ECRH systems up to 1.5 MW as well as current drive (25 kA at $n_{e0} = 8 \times 10^{19}\,\mathrm{m}^{-3}$). Mitigation of disruptions with on-axis ECRH appears promising. Effective synergy between EC waves and LHCD has been used to produce e-ITBs at high density and high plasma current at magnetic fields for which the 'cold' EC resonance is outside the plasma.

A prototype ITER-relevant LHCD launcher—the PAM—has been successfully tested ($f = 8$ GHz), and shows high power handling, good coupling properties and current drive effects comparable to those of a conventional launcher. Electron ITBs have been produced at high density in FTU with the combined use of LHCD and ECRH: $T_{i0} = 6$ keV with $n_{e0} = 1.4 \times 10^{20}\,\mathrm{m}^{-3}$ and $H_{97} = 1.6$. Turbulence is strongly reduced. Ions are heated by collisions with $\Delta T_i / T_i$ up to 35% showing that e-ITBs are not degraded by the electron–ion collisions. Particle pinch studies have been made at high densities in full current drive conditions where the Ware pinch plays no role, confirming the presence of an anomalous inward pinch at high densities ($n_{e0} = 1.5 \times 10^{20}\,\mathrm{m}^{-3}$).

FTU will resume operation in 2005 with the exploitation of the LHCD, the ECRH and the IBW systems at their full power capability. Active control of MHD (tearing modes) with ECRH is being prepared. A more systematic study of disruption mitigation will be done by triggering the EC power at the time of the change of V_{loop} associated with the start of the disruption. It is also planned to install an active beam diagnostic system with the aim of measuring ion temperature profiles and also the current profile through motional Stark effects (MSEs). Installation of a lithium limiter is also planned, in collaboration with the TRINITI Institute (Russia), where the lithium diffuses through capillarity allowing different conditioning techniques (boronization, titanization, etc) to be compared. Assessment of the capability of such a capillary system to withstand the electromagnetic forces in a tokamak and, therefore, avoiding pollution from lithium droplets, will be attempted.

On a longer timescale, the conceptual study for a substantial upgrade of FTU in an 8 T/6 MA machine (FT3) has been finalized [48]. FT3 would aim at achieving burning plasma conditions in deuterium plasmas with the alpha particle dynamics simulated by fast ion tails produced by ICRH (at a power level of about 20 MW) in order to provide an important contribution to the accompanying programme to ITER.

References

[1] C. Gormezano (Guest ed) 2004 Special issue on FTU *Fusion Sci. Technol.* **45**

[2] Angelini B. *et al* 2003 *Nucl. Fusion* **43** 1632–40

[3] Vershkov V.A., Dreval V.V. and Soldatov S.V. 1999 *Rev. Sci. Instrum.* **70** 1700

[4] Vershkov V.A. *et al* 2001 First results of turbulence measurements in FTU with heterodyne correlation reflectometer *28th EPS Conf. on Plasma Physics (Madeira, 2001)* P1.011

[5] Tudisco O. *et al* 2004 *Fusion Sci. Technol.* **45** 402

[6] Bibet Ph. *et al* 1994 *Rep. EUR-CEA-FC-1520* CEN Cadarache, France

[7] Mirizzi F. *et al* 2003 Experiment with the PAM launcher for FTU *20th Symp. on Fusion Engineering (SOFE 2003) (San Diego, CA, October 2003)* at press

[8] ITER Physics Basis 1999 *Nucl. Fusion* **39** chapter 6, 2495 and references therein

[9] Pericoli Ridolfini V. *et al* 2004 Experimental test of an ITER-like passive active multijunction lower hybrid RF launcher on the FTU tokamak *31st EPS Conf. on Plasma Physics (London, 28 June–2 July 2004)* P2–105

[10] Pericoli Ridolfini V. *et al* 2004 *Proc. 20th Fusion Energy Conf. (Vilamoura, Portugal, 2004)* IAEA-EX/5-5, http://www-naweb.iaea.org/napc/physics/fec/fec2004/datasets/index.html

[11] Esterkin A.R. and Piliya A.D. 1996 *Nucl. Fusion* **38** 1501

[12] Barbato E. *et al* 2004 *Fusion Sci. Technol.* **45** 323

[13] Karney C.F.F. and Fisch N.J. 1985 *Phys. Fluids* **28** 116

[14] Tala T.J.J. *et al* 2000 *Nucl. Fusion* **40** 1635

[15] Barbato E. and Saviliev A. 2004 Benchmarking of LHCD numerical modelling on FTU discharges and application to ITER-FEAT scenarios *31st EPS Conf. on Plasma Physics (London, 28 June–2 July 2004)* P2-104

[16] Bonoli P. *et al* 2003 *Radio Frequency Power in Plasmas* ed C.B. Forest (New York: AIP) *AIP Conf. Proc.* **694** 24

[17] Granucci G. *et al* 2004 *Fusion Sci. Technol.* **45** 387

[18] James R.A. *et al* 1992 *Phys. Rev.* A **45** 8783

[19] Nowak S., Lazzaro E. and Ramponi G. 1996 *Phys. Plasmas* **3** 4140

[20] Martin-Solis J.R. *et al* 2004 *Nucl. Fusion* **44** 974

[21] Castaldo C. *et al* 2004 *Nucl. Fusion* **44** L1–4

[22] De Benedetti M. *et al* 2004 *Proc. Conf. on Plasma Physics (London, 28 June–2 July 2004)*

[23] Vershkov V.A. *et al* 1997 *Proc. Int. Conf. on Fusion Energy (Montreal, 1996)* vol 1 (Vienna: IAEA) p 519

[24] Vershkov V.A. *et al* 1999 *Nucl. Fusion* **39** 1775

[25] Frigione D. *et al* 2001 *Nucl. Fusion* **41** 1613

[26] Giovannozzi E. *et al* 2004 *Nucl. Fusion* **44** 226

[27] Annibaldi S.V. *et al* 2004 *Nucl. Fusion* **44** 12

[28] Frigione D. *et al* 2004 Pellet injection from the high field side on FTU *31st EPS Conf. on Plasma Physics (London, 28 June–2 July 2004)* P-2.101

[29] Giovannozzi E. *et al* 2004 *Proc. 20th Fusion Energy Conf. (Vilamoura, Portugal, 2004)* IAEA-EX/P4-4, http://www-naweb.iaea.org/napc/physics/fec/fec2004/datasets/index.html

[30] Romanelli M. *et al* 2004 *Proc. 20th Fusion Energy Conf. (Vilamoura, Portugal, 2004)* IAEA-EX/P6-24, http://www-naweb.iaea.org/napc/physics/fec/fec2004/datasets/index.html

[31] Castaldo C. *et al Nucl. Fusion* submitted

[32] Cenacchi G. and Taroni A. 1988 *JETTO: A Free Boundary Plasma Transport Code* ENEA/TIB/88/5, ENEA

[33] Esposito B. *et al* 2004 *Plasma Phys. Control. Fusion* **46** 1793–804

[34] Pericoli Ridolfini V. *et al* 2003 *Nucl. Fusion* **43** 469

[35] Tresset G. *et al* 2002 *Nucl. Fusion* **42** 520

[36] Shelukhin D.A., Vershkov V.A. and Razumova K.A. 2004 Turbulence suppression in discharges with off-axis ECRH in T-10 *Proc. 20th Fusion Energy Conf. (Vilamoura, Portugal, 2004)* IAEA-EX/P6-26, http://www-naweb.iaea.org/napc/physics/fec/fec2004/datasets/index.html

[37] Gormezano C. *et al* 2003 High density electron transport barriers in the FTU tokamak *30th EPS Conf. on Plasma Physics (St Petersburg, 7–11 July 2003)* P2-145

[38] Frigione D. *et al* 2004 *Fusion Sci. Technol.* **45** 339
[39] Hassam A.B. *et al* 1990 *Phys. Fluids* B **2** 1822
[40] Romanelli F. and Zonca F. 1993 *Phys. Fluids* B **6** 4081
[41] Garbet X. *et al* 2003 *Phys. Rev. Lett.* **91** 035001
[42] Hoang G.T. *et al* 2003 *Phys. Rev. Lett.* **90** 155002
[43] Jacquinot J. *et al* 2004 *Proc. 20th Fusion Energy Conf. (Vilamoura, Portugal, 2004)* IAEA-OV/2-2, http://www-naweb.iaea.org/napc/physics/fec/fec2004/datasets/index.html
[44] Buratti P. *et al* 2004 *Proc. 20th Fusion Energy Conf. (Vilamoura, Portugal, 2004)* IAEA-EX P5-1, http://www-naweb.iaea.org/napc/physics/fec/fec2004/datasets/index.html
[45] Chu M.S., Greene J.M., Lao L.L., Turnbull A.D. and Chance M.S. 1992 *Phys. Fluids* B **4** 3713
[46] Kieras C.E. and Tataronis J.A. 1982 *J. Plasma Phys.* **28** 395
[47] Zonca F., Chen L. and Santoro R.A. 1996 *Plasma Phys. Control. Fusion* **38** 2011
[48] Romanelli F. *et al* 2004 *Fusion Sci. Technol.* **45** 483